HHS Public Access

Author manuscript

Oncogene. Author manuscript; available in PMC 2023 May 18.

Published in final edited form as:

Oncogene. 2023 March ; 42(13): 1038–1047. doi:10.1038/s41388-023-02620-x.

Runx1/3-driven adaptive endoplasmic reticulum stress pathways contribute to neurofibromagenesis

Youjin Na[1], **Ashley Hall**[1], **Yanan Yu**[1,6], **Liang Hu**[1], **Kwangmin Choi**[1], **Jake A. Burgard**[1], **Sara Szabo**[2], **Gang Huang**[3,4], **Nancy Ratner**[1,5], **Jianqiang Wu**[1,5]

[1]Division of Experimental Hematology and Cancer Biology, Cancer & Blood Diseases Institute, Cincinnati Children's Hospital Medical Center, 3333 Burnet Ave, Cincinnati, OH 45229, USA.

[2]Department of Pediatrics and Department of Pediatric Pathology, Cincinnati Children's Hospital Medical Center, University of Cincinnati, Cincinnati, OH, USA.

[3]Department of Cell Systems & Anatomy and Department of Pathology & Laboratory Medicine, UT Health San Antonio, Joe R. and Teresa Lozano Long School of Medicine, Mays Cancer Center at UT Health San Antonio, San Antonio, TX, USA.

[4]Department of Pathology & Laboratory Medicine, UT Health San Antonio, Joe R. and Teresa Lozano Long School of Medicine, Mays Cancer Center at UT Health San Antonio, San Antonio, TX 78229, USA.

[5]Department of Pediatrics, University of Cincinnati College of Medicine, Cincinnati, OH 45267, USA.

[6]Present address: College of Life Science, Xuzhou Medical University, 221004 Jiangsu, P. R. China.

Abstract

Neurofibromatosis type 1 (NF1) patients are predisposed to develop plexiform neurofibromas (PNFs). Three endoplasmic reticulum (ER) stress response pathways restore cellular homeostasis. The unfolded protein response (UPR) sensors contribute to tumor initiation in many cancers. We found that all three UPR pathways were activated in mouse and human PNFs, with protein kinase RNA [PKR]-like ER kinase (PERK) the most highly expressed. We tested if neurofibroma cells adapt to ER stress, leading to their growth. Pharmacological or genetic inhibition of PERK reduced mouse neurofibroma-sphere number, and genetic inhibition in PERK in Schwann cell precursors (SCPs) decreased tumor-like lesion numbers in a cell transplantation model. Further, in a PNF mouse model, deletion of PERK in Schwann cells (SCs) and SCPs reduced tumor size, number, and increased survival. Mechanistically, loss of *Nf1* activated

Correspondence and requests for materials should be addressed to Jianqiang Wu. Jianqiang.wu@cchmc.org.

AUTHOR CONTRIBUTIONS

GH, NR, and JW designed analyses, and discussed results. YN, AH, YY, LH and JAB performed experiments. KC performed bioinformatic analysis. SS reviewed the slides. YN, GH, NR, and JW wrote and edited the paper.

COMPETING INTERESTS

The authors declare no competing interests.

Supplementary information The online version contains supplementary material available at https://doi.org/10.1038/s41388-023-02620-x.

PERK-eIF2α-ATF4 signaling and increased ATF4 downstream target gene p21 translocation from nucleus to cytoplasm. This nucleus-cytoplasm translocation was mediated by exportin-1. Runx transcriptionally activated ribosome gene expression and increased protein synthesis to allow SCs to adapt to ER stress and tumor formation. We propose that targeting proteostasis might provide cytotoxic and/or potentially durable novel therapy for PNFs.

INTRODUCTION

Neurofibromatosis type 1 (NF1) is an autosomal dominantly inherited human disorder affecting ~1 in 2500 births [1, 2]. NF1 is caused by mutations in the tumor suppressor gene NF1 that encodes neurofibromin, a negative regulator of the Ras pathway [3-5]. Loss of function NF1 leads to RAS-MAPK pathway activation, cell proliferation, tumor formation, and growth in the nervous system [5]. Most of NF1 patients (95%) are predisposed to dermal neurofibromas (DNF) and/or plexiform neurofibromas (PNF) [5, 6]. Underlying mechanism(s) of tumorigenesis are not fully understood.

The endoplasmic reticulum (ER) is an essential organelle in eukaryotic cells. Induction of ER stress leads to the unfolded protein response (UPR). There are three known UPR pathways: PERK, IRE-1α, and ATF6. All three pathways mediate stress-induced physiological UPR adaptive response that maintains normal cell function by regulating proteostasis—specifically, decreasing protein synthesis and increasing ER protein folding capacity, autophagy, and proteasome-dependent ER-associated degradation (ERAD) of misfolded proteins [7-9]. Thus, proteostasis regulates the ER stress response and UPR, which itself feeds back to regulate proteostasis. When ER stress cannot be resolved, UPR signaling induces either apoptosis or autophagy [10]. Thus, UPR can pivot between promoting cell survival and promoting cell death. Tumor cells can exploit UPR signaling to promote their survival and progression [8, 11, 12]. Indeed, the entire proteostasis-mediated ER stress/UPR response axis is critical in cancer cells [13, 14]. In fact, in *Nf1*$^{-/-}$ MPNST, further elevation of increased ER stress signaling causes cell death and reduces tumor growth in vivo [15]. However, ER stress signaling remains unstudied in benign PNFs.

Molecular drivers of ER stress signaling have been well studied in normal and tumor cells but not in PNFs. Reports show that all three ER stress pathways function in tumor progression [8, 16]. PERK also plays an important role in tumor initiation in models of Ras-transformed melanoma [17] and Ret-induced fibroblast transformation [18]. The role of PERK in PNF formation and/or growth has not been studied. In this study, we show that all three ER stress pathways' signalings are elevated, with PERK expression the highest. Loss of *Nf1* activated PERK-eIF2α-ATF4 signaling and increased ATF4 regulated p21 translocation from nucleus to cytoplasm to contribute to neurofibroma formation. This nucleus-cytoplasm translocation was mediated by exportin-1. Further, the RUNX transcription factor mediates proteostasis to adapt UPR to support SC survival and the following PNF formation.

RESULTS

ER stress pathways are activated in mouse and human PNFs

We previously showed that Runx1/3 contributes to PNF formation by transcriptionally and translationally repressing PMP22 expression. KEGG pathway analysis on a RNA-seq data set of genes that are differentially expressed in PNFs from *Runx1*$^{fl/fl}$*;Runx3*$^{fl/fl}$*;Nf1*$^{fl/fl}$*;DhhCre* vs *Nf1*$^{fl/fl}$*;DhhCre* mice showed that the ER stress signalling pathway ("protein process in ER") was the top deregulated pathway [19]. To test if Runx might regulate protein synthesis to adapt to ER stress signalling in PNFs, we performed a retrospective analysis on our published human and mouse PNF microarray data (GSEA14038) [20] and found that expression of genes in all three major ER stress pathways was significantly increased in both (Fig. 1A, B). Consistently, Western blots showed increased expression of ER stress-related proteins in DRG dissected from 1-month-old *Nf1*$^{fl/fl}$*;DhhCre* mice (before tumor formation) and in PNFs from 7-month-old *Nf1*$^{fl/fl}$*;DhhCre* mice (tumor developed), compared to WT control DRGs (Fig. 1C).

PERK expression is increased in mouse and human PNFs and appears to be partially MEK/ERK and RUNX1/3 dependent

Multiple studies suggest that PNFs are derived from SCs [21-24]. In fluorescence-activated cell sorting (FACS) SCs (*p75*$^{+}$*/CD31*$^{-}$*/CD11b*$^{-}$*/CD11b*$^{-}$) isolated from DRG and PNFs dissected from 1- and 7- month-old *Nf1*$^{fl/fl}$*;DhhCre* mice, we identified 1386 differentially expressed genes, using a twofold difference threshold (*t*-test, $P < 0.05$) [25]. Eif2ak3 (Perk) was the only ER stress pathway-related gene exhibiting this degree of differential expression (Fig. 2A). In mouse tissue, Western blotting confirmed increased expression of PERK signaling pathway components (i.e., PERK, p-PERK, p-eIF2α, and ATF4) vs WT controls (Fig. 2B). We validated this finding in human tissue, finding that PERK immunolabelling was elevated in PNF (vs normal nerve control; Fig. 2C).

Sustained MEK/ERK signaling contributes to NF1 tumor formation and growth in human and mouse PNFs, and the treatment of MEK inhibitor, PD0325901, delays tumor growth and reduces cell proliferation [26]. To determine if MEK modifies ER stress signaling in PNF SCs, we treated the *Nf1*$^{fl/fl}$*;DhhCre* PNF mice with MEKi (vs control) by oral gavage for 5 days (PD0325901,1.5 mg/kg/day); Western blots revealed reduced p-ERK1/2, and reduction of all three ER stress pathway proteins (i.e., PERK, IRE1α, and ATF6). Consistently, p-eIF2α expression was increased (Fig. 2D). Thus, all three UPRs showed decreased expression compared to the vehicle control, suggesting that these UPRs, including PERK signaling, might be partially MEK-dependent. PERK signaling is an important downstream pathways of UPR and often activated in cancer cells, but the role of PERK in neurofibroma formation is not clear. Therefore, we focused on the function of the PERK pathway in neurofibromas for further study.

To determine if Runx1/3 modulates ER stress signaling in our system, we performed qRT-PCR to assay expression of the ER stress-related genes *Grp78, Xbp-1, Perk*, and *Atf6* in PNFs from *Runx1*$^{fl/fl}$*;Runx3*$^{fl/fl}$*;Nf1*$^{fl/fl}$*;DhhCre* (vs *Nf1*$^{fl/fl}$*;DhhCre*) mice. All four genes were significantly downregulated in the *Runx1*$^{fl/fl}$*;Runx3*$^{fl/fl}$*;Nf1*$^{fl/fl}$*;DhhCre* (Fig. 2E).

Western blot data revealed that both PERK and ATF4 protein expression were decreased in *Runx1*$^{fl/fl}$;*Runx3*$^{fl/fl}$;*Nf1*$^{fl/fl}$;*DhhCre* PNFs (Fig. 2F).

Pharmacological and genetic inhibition of PERK decreases mouse SCPs and neurofibroma sphere number in vitro

To test if inhibition of PERK affects SCP growth and/or tumorigenesis, we used a neurofibroma sphere culture system, in which SCPs grow as self-renewing spheres that can be passaged in vitro [27]. We used embryonic day 12.5 (E12.5) WT mouse DRG spheres and E12.5 *Nf1*$^{-/-}$ mouse DRG spheres for initial testing. We confirmed PERK signalling is activated in *Nf1*-deficient SCP spheres compared to wild-type spheres (Fig. S1A). To determine whether PERK inhibition affects SCP proliferation, we treated E12.5 WT and *Nf1*$^{-/-}$ DRG spheres with GSK2606414 [28], a highly selective PERK inhibitor (PERKi). GSK2606414 inhibited sphere formation in a dose-dependent manner in both WT and *Nf1*$^{-/-}$ DRG spheres; *Nf1*$^{-/-}$ spheres showed tenfold higher drug sensitivity than WT spheres (Fig. S1B), suggesting that GSK2606414 has differential inhibitor effects on WT and *Nf1*$^{-/-}$ Schwann cell precursors. To determine if PERK is relevant to SCP growth or tumor formation upon loss of *Nf1*, we used secondary mouse PNF-derived sphere cultures. GSK2606414 inhibited sphere formation in a dose-dependent manner (Fig. 3A). The inhibitory effect of PERK by GSK2606414 on spheres was confirmed by Western blot; 10 μM and 50 μM PERKi decreased levels of PERK, increased levels of p-eIF2α (suggesting that protein synthesis decreased), and increased levels of CHOP (i.e., induced apoptosis) (Fig. 3B). A time course showed that 10 uM GSK2606414 inhibited PERK until 6 h, and simultaneously activated apoptotic markers such as cleaved PARP and Chop; this inhibitory effect disappeared after 24 h (Fig. 3C).

To test if the inhibitory effect was specifically caused by PERK, we treated *Nf1*$^{fl/fl}$;*DhhCre* mouse DRG/neurofibroma-derived spheres with two different Perk sh-RNAs (sh*Perk*) for 4 days. Treatment significantly decreased sphere numbers compared to the non-target (sh*NT*) control (Fig. 3D). Perk knockdown was confirmed by Western blot (Fig. 3E).

PERK contributes to neurofibroma growth

To test whether PERK reduction in neurofibroma sphere numbers decreases tumorigenic potential, we injected sh*Perk* or sh*NT* lentivirus-treated *Nf1*$^{fl/fl}$;*DhhCre* mouse DRG/neurofibroma-derived sphere cells subcutaneously into nude mice (*nu/nu*). Two months after transplantation, 8 of 10 *nu/nu* mice grafted with sh*NT*-treated spheres showed neurofibroma-like micro-lesions, while fewer lesions (2 of 10 *nu/nu*) were detected in mice grafted with sh*Perk*-treated spheres ($p < 0.05$) (Fig. 3F). These data suggest that PERK might contribute to neurofibroma growth.

Targeted genetic deletion of *Perk* increases survival; decreases tumor number and size in the *Nf1*$^{fl/fl}$;*DhhCre* PNF mouse

We next tested whether targeted genetic deletion of PERK in SCs and SCPs in *Nf1*$^{fl/fl}$;*DhhCre* mice affects PNF formation. We carried out survival analysis. Based on the previous statistical analysis, we used 20 mice per group for comparison. Kaplan–Meier analysis revealed a significant survival difference between *Perk*$^{fl/fl}$;*Nf1*$^{fl/fl}$;*DhhCre* mice

and littermate *Perk*$^{fl/+}$;*Nf1*$^{fl/fl}$;*DhhCre* mice ($p < 0.05$) (Fig. 4A). However, because of the breeding strategy, we could not obtain littermates *Nf1*$^{fl/fl}$;*DhhCre* for direct comparison. Similar significance was detected on survival time between *Perk*$^{fl/fl}$;*Nf1*$^{fl/fl}$;*DhhCre* and previously published *Nf1*$^{fl/fl}$;*DhhCre* mice [21] (not shown), suggesting that PERK contributed to PNF initiation and tumor growth, but the loss of one allele of PERK might not change tumor penetration rate.

We previously showed that in the *Nf1*$^{fl/fl}$;*DhhCre* model, each mouse develops 4–20 neurofibromas [21]. We hypothesized that if PERK contributes to neurofibroma initiation, then tumor number should be reduced in *Perk*$^{fl/fl}$;*N*$^{f1fl/fl}$;*DhhCre* mice. Indeed, gross dissections of 5 month-old mice showed that *Perk*$^{fl/fl}$;*Nf1*$^{fl/fl}$;*DhhCre* mice had significantly fewer spinal cord tumors/mouse vs age matched *Perk*$^{fl/+}$;*Nf1*$^{fl/fl}$;*DhhCre* littermates (Fig. 4B, C). Neurofibroma diameter measured on spinal root dissected sections confirmed significantly smaller tumors (Fig. 4B, D). At 12 months of age, we counted mouse neurofibroma number and measured tumor diameters;both were significantly different in *Perk*$^{fl/fl}$;*Nf1*$^{fl/fl}$;*DhhCre* vs *Perk*$^{fl/+}$;*Nf1*$^{fl/fl}$;*DhhCre* littermate controls (Fig. 4E, F), suggesting PERK might contribute to PNF growth. H&E staining showed that all tumors were still GEM-grade 1 neurofibroma (not shown). Ki67^{+}-proliferating cell numbers in neurofibroma tissue sections were significantly decreased in *Perk*$^{fl/fl}$;*Nf1*$^{fl/fl}$;*DhhCre* neurofibromas compared to *Perk*$^{fl/fl}$;*Nf1*$^{fl/fl}$;*DhhCre* neurofibromas compared to *Perk*$^{fl/+}$;*Nf1*$^{fl/fl}$;*DhhCre* mouse tumors (Fig. 4G, H). There was no difference in cell death as determined by TUNEL staining (average 1–2% in both genotypes, not shown). Therefore, glial cell PERK regulates *Nf1*-deficient tumor cell proliferation in neurofibromas, and co-activation of PERK in SCs and/or SCPs is important for neurofibroma initiation and growth. We only detected mild prolonged survival by loss of both Perk alleles in the *Nf1*$^{fl/fl}$;*DhhCre* model (Fig. 4A), suggesting that Perk might not play a dominant role, or the other two ER stress pathways might compensate the stress signaling upon conditional loss of Perk in PNF formation. To determine the potential causes, we performed qRT-PCR on tumors from *Perk*$^{+l+}$;*Nf1*$^{fl/fl}$;*DhhCre*, *Perk*$^{fl/+}$;*Nf1*$^{fl/fl}$;*DhhCre*, and *Perk*$^{fl/fl}$;*Nf1*$^{fl/fl}$;*DhhCre*. *Perk* RNA expression remained relative low level in *Perk*$^{fl/fl}$;*Nf1*$^{fl/fl}$;*DhhCre* mouse tumors, but not in *Perk*$^{fl/+}$;*Nf1*$^{fl/fl}$;*DhhCre* tumors compared to *Perk*$^{+l+}$;*Nf1*$^{fl/fl}$;*DhhCre* tumors. We detected increased expression of *Xbp-1*, a substrate of IRE1a pathway, although no statistical difference was detected. *Grp78* was relative high because it is involved in all 3 ER stress pathway. *Atf6* expression varied but remained similar levels in all 3 genotypes (Fig. 4J). We then performed Western blots on tumors from the above genotypes. We detected decrease PERK protein expression in *Perk*$^{fl/fl}$;*Nf1*$^{fl/fl}$;*DhhCre* tumors compared to other two genotypes. Although the protein expression levels varied due to primary tumor variation, we detected increased IRE1a expression in 2 of 3 *Perk*$^{fl/fl}$;*Nf1*$^{fl/fl}$;*DhhCre* mouse tumors compared to *Perk*$^{+l+}$;*Nf1*$^{fl/fl}$;*DhhCre* controls (Fig. 4K). In combined with RNA expression data, these results suggest IRE1α might compensate the ER stress pathway to maintain the tumor growth.

Total p21 and cytoplasmic p21 expressions are increased in mouse and human PNFs

Data in Figs. 1-4 suggested that the loss of Nf1 activated PERK-eIF2α-ATF4 signaling might adapt to the stressful tumor environment enabling SC survival and PNF formation.

We therefore investigated the downstream effectors of ATF4 in the PERK pathway involving a pro-survival signalling in PNFs. Recent studies showed that cyclin-dependent kinase inhibitor p21 is a target gene of *ATF4* [29] and loss of *Nf1 in* fibroblast cells upregulated p21 by an unknown mechanism [30]. P21 acts not only as a tumor suppressor but also may play an oncogenic role involving nucleus-cytoplasmic translocation [31, 32]. Western blots showed that total p21 and phosphor-p21 (detecting cytoplasmic p21) protein expression was increased in PNFs compared to controls (Fig. 5A). Consistently, ATF4 expression was also increased in PNFs. IHC staining showed increased p21 expression in $Nf1^{fl/fl}$;*DhhCre* mouse PNFs compared to WT DRG control (Fig. 5B). We also performed immunofluorescence staining on mouse and human PNF-derived SCs to investigate the expression levels of cytoplasmic p21. We detected significantly augmented cytoplasmic p21 as well as total p21 expression in 7 months mouse PNF-derived SCs compared to WT mouse SCs (Fig. 5C). Similarly, immunofluorescence staining showed increased cytoplasmic p21 and total p21 expression in human PNFs compared to normal human nerve controls (Fig. 5D, E).

ATF4 binds to p21 (Cdkn1a) intron 1 region to regulate p21 expression in PNFs

To determine if p21 might be directly upregulated by ATF4, we performed an in silico search for potential ATF4 binding sites. We identified two sites in the mouse p21 (*Cdkn1a*) intron region 1 (Supplemental Fig. 2A). To confirm the relevance of these sites, $Nf1^{fl/fl}$;*DhhCre* PNF DNA was subjected to ChIP using an anti-ATF4 antibody. We confirmed ATF4 binding to p21 at the intron 1 region by PCR (Supplemental Fig. 2B), consistent with p21 being directly activated by ATF4. We also tested if ATF4 regulates p21 nucleus-cytoplasmic translocation. We treated $Nf1^{fl/fl}$;*DhhCre* mouse PNF-derived spheres with two shATF4, Western blots of lysates from these cells showed that reduced ATF4 correlated with decreased cytoplasmic p21 (p-p21) expressions, but minor changes in total p21 (p21) (Supplemental Fig. 2C). These results suggest that p21 is a potential target of *ATF4*, and increased ATF4 regulated p21 translocation from nucleus to cytoplasm.
To determine the correlation between Perk and p21, we then performed immunostaining on tumors from $Perk^{+/+}$;$Nf1^{fl/fl}$;*DhhCre* and $Perk^{fl/fl}$;$Nf1^{fl/fl}$;*DhhCre* mouse. We detected significantly increased nucleic p21 and decreased cytoplasmic p21 expression in $Perk^{fl/fl}$;$Nf1^{fl/fl}$;*DhhCre* tumors compared to tumors from $Perk^{+/+}$;$Nf1^{fl/fl}$;*DhhCre* mouse (Fig. 5G, H), suggesting *Perk* change correlates to p21 nucleus-cytoplasmic translocation.

Exportin-1 mediates p21 nucleus-cytoplasmic translocation

Nucleus-cytoplasmic export is mainly regulated by Exportin-1(XPO-1, also known as CRM1) [33]. We tested if p21 and XPO-1 interact by performing p21-pull down assays. Anti p21-pulled down XPO-1 (Fig. 6A), suggesting that p21 and XPO-1 might interact. Also, XPO-1 expression and cytoplasmic p21 expression were elevated in human PNF tissue sections vs normal nerve controls. Elevated levels of nuclear XPO-1 and p21 in normal human nerve, and higher level of cytoplasmic p21 in human PNFs, suggest that XPO-1 is involved in p21 translocation from nucleus to cytoplasm in PNFs (Fig. 6B).

To test if blockade of nuclear export XPO-1 affects p21 locally action, we treated $Nf1^{fl/fl}$;*DhhCre* mouse PNF-derived spheres with KPT-330, a selective inhibitor of nuclear export (SINE). KPT-330 inhibited sphere number in a dose-dependent manner (Fig. 6C).

In a time course (5 μM treatment), cytoplasmic p-p21 levels gradually reduced until 12 h, and XPO-1 expression was maintained in the nucleus (Fig. 6D). These results indicate that nuclear-cytoplasmic translocation of p-p21 depends on XPO-1 expression.

Runx1/3 transcriptionally activates ribosome gene expression

To determine if Runx might regulate protein synthesis in Nf1 SCs, we performed gene ontology analysis using published Runx1 ChIP-seq peaks of genes within 10 kb of Runx1-binding sites (GSE122775) [19] The top results for functional annotations of "cellular component" and "molecular function" revealed ribosomal involvement (Fig. 7A, B). We re-analyzed RNA-seq differential expression data of PNFs from *Nf1$^{fl/fl}$;DhhCre* vs *Runx1$^{fl/fl}$;Runx3$^{fl/fl}$;Nf1$^{fl/fl}$;DhhCre* mice (GSE122774 [19], and found 11 of the hits were ribosomal genes (Fig. 7C). QRT-PCR revealed that most were significantly reduced in *Runx1$^{fl/fl}$;Runx3$^{fl/fl}$;Nf1$^{fl/fl}$;DhhCre* PNFs. In contrast, ribosomal genes that are not targets of Runx (i.e., not shown in CHIP-seq) exhibited increased expression or no change (Fig. 7D). We assayed nascent protein synthesis using nascent protein synthesis assayed with a Click-iT Protein Synthesis Assay Kit. Protein synthesis was high in PNF SCs from *Nf1$^{fl/fl}$;DhhCre* mice, but significantly decreased in SCs derived from PNFs of the *Runx1$^{fl/fl}$;Runx3$^{fl/fl}$;Nf1$^{fl/fl}$;DhhCre* mice, reaching levels not significantly different from WT SCs (Fig. 7E, F). Together, these data support the idea that Runx transcription factors regulate protein synthesis in Nf1 mutant SCs.

DISCUSSION

Tumor development is due to dysregulated tumor cell proliferation and other environmental stressors which can induce abnormal protein synthesis, resulting in the accumulation of misfolded or unfolded proteins in the ER lumen. ER stress, especially ERAD, maintains proteostasis so that tumor cells adapt to stressful conditions for survival. Thus activated UPR signaling has been reported in various types of cancer, and the ability to tolerate persistent ER stress enhances cancer cell survival, metastasis, drug resistance, and immunosuppressive effects [8]. ER stress response plays pivotal roles in tumor initiation and/or growth in multiple cancers—including brain, breast, gastric, kidney, liver, lung, and pancreatic [34-36]. ER stress signaling has also been extensively studied in SC biology or pathology. For example, in a mouse model of Charcot-Marie-Tooth disease, UPR is activated in myelinating SCs, suggesting that ER stress plays a role in this peripheral neuropathy [37, 38]. In this study, we showed that all three UPR pathways were activated in mouse and human PNFs. Loss of Nf1 activated PERK-eIF2 α-ATF4 signaling, and increased ATF4 regulated p21 translocation from nucleus to cytoplasm that was mediated by exportin-1. Mechanistically, Runx1/3 activated ribosome gene expression and increased protein synthesis to allow cells to adapt to ER stress. We detected the expression of ER stress-related genes, *Grp78, Xbp-1, Perk, and Atf6* in PNFs from *Runx1$^{fl/f}$;Runx3$^{fl/fl}$;Nf1$^{fl/fl}$;DhhCre* were significantly downregulated compared to those from *Nf1$^{fl/fl}$;DhhCre* mice. However, the results do not necessarily indicate that the downregulation of these ER stress signaling genes is directly regulated by Runx1/3, but instead can be caused by indirect effects due to Runx1/3 loss-induced tumor inhibition. Similarly, the inhibitory effects on ER stress-related protein expression by MEKi can also be the indirect effects on the ER stress signaling pathways.

While all 3 ER stress pathways function in tumor formation, PERK plays a dominant role in tumor initiation in models of Ras-transformed melanoma [17] and Ret-induced fibroblast transformation [18]. PERK also promotes breast cancer growth as PERK loss-of-function leads to smaller tumors and increased survival [39, 40]. In addition, PERK pharmacological inhibition reduced breast cancer metastasis [41]. Consistent with these reports on cancer, we showed that Perk contributed to PNF initiation in an in vivo cell transplantation mouse model and in the *Nf1*$^{fl/fl}$*;DhhCre* genetically engineered mouse model. Further, our in vitro results on SCs protein synthesis (Fig. 7E, F) suggest that PERK might also contribute to tumor growth. However, we only detected mild prolonged survival by loss of both Perk alleles in the *Nf1*$^{fl/fl}$*;DhhCre* model (Fig. 4A). There are several possibilities: (1) Compensatory ER stress pathway, such as IRE1α, might be involved upon conditional loss of PERK. (2) Perk might only play a minor role in PNF formation, (3) other pathway might contribute to PNF formation.

The cyclin-dependent kinase inhibitor p21 acts not only as a tumor suppressor but also plays an oncogenic role as an inhibitor of apoptosis [31, 32]. This oncogenic p21, located in the cytoplasm, and elevated cytoplasmic p21 are critical for promoting cell transformation and tumor progression. The cytoplasmic localization of p21 arises from phosphorylation of Thr145, located in the nuclear localization signal (NLS) of p21. Phosphorylated p21 (p-p21) shuttles between the nucleus and the cytoplasm are more stable in cancers, therefore maintain elevated level of p-p21 in cytoplasm [31, 42, 43]. Up-regulated p21 in *Nf1*-knockdown human fibroblasts treated with Nf1-specific shRNA has been reported [30]. We showed increased p-p21 (cytoplasmic p21), as well as total p21 expression, in mouse and human PNFs (Fig. 5C, D). We also show increased nucleic p21 and decreased cytoplasmic p21 expression in *Perk*$^{fl/fl}$*;Nf1*$^{fl/fl}$*;DhhCre* tumors compared to tumors from *Perk*$^{+/+}$*;Nf1*$^{fl/fl}$*;DhhCre* mouse (Fig. 5G,H). However, what we detected is the correlation between PERK-elF2α-ATF4 and its downstream target p21. Whether p21 plays a functional role in PNF formation is not directly tested. It will be interesting to test if knock out of p21 in *Nf1*$^{fl/fl}$*;DhhCre* mice will change PNF number and grade.

Nuclear-cytoplasmic export is mainly regulated by XPO-1, the sole nuclear exporter of tumor-suppressors and growth-stimulatory proteins [33]. Disrupted and aberrant expression of XPO-1 is frequently observed in cancer cells, and the subsequent translocalization of these key regulatory proteins contribute to cell survival, tumorigenesis, and tumor progression [44]. We showed that p21 translocation is XPO-1 dependent, and that XPO-1 regulates p21 nucleus-cytoplasm translocation in PNF cells. These results suggest that inhibition XPO-1 might provide a potential therapy for PNFs.

The ribosome is responsible for protein synthesis, and an increase in synthesized protein results in the activation of ER stress and UPR. Interestingly, Runx1 regulates ribosomal gene transcription by binding to the promoters of ribosomal genes [45]. A recent study showed that loss of *Runx1* attenuates UPR signaling and lower protein synthesis and increases ER stress resistance along with markedly reduced ribosome biogenesis in hematopoietic stem and progenitor cells (HSPCs), where Runx1 serves as a tumor suppressor [46]. We previously demonstrated that Runx1 functions as an oncogene in PNFs, and that loss of *Nf1* induces *Runx1* overexpression but not Runx3 in mouse PNFs [47].

However, conditional knockout of Runx1 only transiently delayed neurofibroma growth and induced compensatory overexpression of Runx3 in the *Runx1*$^{fl/fll}$;*Nf1*$^{fl/fl}$;*DhhCre* mouse model. QRT-PCR on *Runx1*$^{fl/fll}$;*Nf1*$^{fl/fl}$;*DhhCre* mouse tumors/DRGs and age-matched *Nf1*$^{fl/fl}$;*DhhCre* tumors indicated that Runx3 expression displayed a pronounced time-dependent increase [19]. Conversely, indeed overexpressed *Runx1* in PNFs increases protein synthesis and UPR signaling to maintain cellular homeostasis in PNF cells. Runx transcriptionally regulated ribosome gene expression and maintained proteostasis. Ribosome RNA sequencing will provide more detail of regulated mRNAs.

In summary, the PERK pathway is a major UPR signal pathway in PNF initiation and is partially regulated by MEK/ERK signaling and RUNX transcription factors. The PERK-eIF2α-ATF4 pathway contributes to PNF and that p21 is a downstream effector of ATF4. Runx1/3 not only serve as oncogene upon loss of *Nf1*, but also are necessary for intrinsic activation of the UPR by enhancing protein synthesis to allow cells to adapt to ER stress (Fig. 7G). Other transcription factors relevant to regulate ATF4 may not be sufficient to drive PNF initiation in vivo. Our results suggest that loss of *Nf1* in SC/SCPs leads to PNF formation by driving Runx1/3, and perhaps other factors regulated proteostasis, to adapt to ER stress signaling. We suggest that targeting this proteostasis mechanism could provide cytotoxic and, thus, potentially durable novel therapy for PNF patients.

MATERIAL AND METHODS

Animals

Mice were housed in temperature- and humidity-controlled facilities on 12 h dark-light cycles with free access to food and water. The animal care and use committees of Cincinnati Children's Hospital Medical Center approved all animal procedures. Institutional Animal Care and Use Committee (IACUC) guidelines were followed with animal subjects. To study the specific function of SCs, we used *DhhCre* transgenic mice, where *Cre*-mediated recombination activity would result in deletion of the floxed Nf1 allele in SCs/SCPs of the developing peripheral nerves at embryonic day 12.5. The *Nf1*$^{fl/fl}$ mouse (*Nf1*$^{fl/fl}$) has been described previously [48] and was on a mixed 129/BL/6 background. The *DhhCre* transgenic mouse line was maintained on C57BL/6. We bred *DhhCre* mice onto *Nf1*$^{fl/fl}$ background to obtain the F1 generation (*Nf1*$^{fl/+}$;*DhhCre*$^{+}$); we bred F1 mice with *Nf1*$^{fl/fl}$ mice to obtain *Nf1*$^{fl/fl}$;*DhhCre* mice.

Breeding *Perk*$^{fl/fl}$;*Nf1*$^{fl/fl}$;*DhhCre* mice: We purchased the C57BL/6 background *Perk*$^{fl/fl}$ mice from the Jackson Laboratory (Maine, NE). We bred the *Perk* $^{fl/fl}$ mice onto the *Nf1*$^{fl/fl}$ mice to obtain F1 generation (*Perk*$^{fl/+}$;*Nf1*$^{fl/+}$). We also bred the *Perk* $^{fl/fl}$ mice with *Nf1*$^{fl/+}$;*DhhCre*$^{+}$ mice to obtain *Perk*$^{fl/+}$;*Nf1*$^{fl/+}$;*DhhCre* mice. We interbred *Perk*$^{fl/+}$;*Nf1*$^{fl/+}$ to obtain *Perk*$^{fl/fl}$;*Nf1*$^{fl/fl}$ mice. We then bred *Perk*$^{fl/fl}$;*Nf1*$^{fl/l}$ with *Perk*$^{fl/+}$;*Nf1*$^{fl/+}$;*DhhCre* mice to obtain *Perk*$^{fl/fl}$;*Nf1*$^{fl/fl}$;*DhhCre* mice. Littermates *Perk*$^{f/l+}$;*Nf1*$^{fl/fl}$;*DhhCre*, or *Perk*$^{fl/fl}$;*Nf1*$^{fl/+}$;*DhhCre* mice were used as controls. Mouse were randomized for survival analysis and the genotypes were blind to investigator. Genotyping was performed as described [21].

Reagents

GSK2606414 (EMD Millipore, Billerica, MA) and KPT-330 (AdooQ® Bioscience, Irvine, CA) were dissolved in dimethyl sulfoxide (DMSO; Sigma-Aldrich). The concentration of DMSO was <0.1% for all experiments to avoid cytotoxicity. CB-5083 (Chemgood, Glen Allen, VA) and PD-0325901 (Pfizer, New York City, NY) were dissolved in 0.5% [w/v] methylcellulose (Sigma-Aldrich, St. Louis, MO) solution with 0.2% [v/v] polysorbate 80 [Tween 80] (Sigma-Aldrich) for mouse dosing.

Mouse embryonic and neurofibroma cell derived sphere treatment

Mouse embryonic and neurofibroma cell derived sphere culture were performed as described [47, 49]. We seeded dissociated single live cells into low attachment plates at a density of 4×10^4 cells/well for 24 h and then incubated with up to 10 μM GSK2606414 or KPT-330 at 37°C. After 4 days, the sphere numbers were counted using phase-contrast microscopy (Olympus CKX41, Tokyo, Japan). For Western blot, 10 uM GSK2606414 or 5 uM KPT-330 were used to treat the spheres (4×10^4 cells/well) for 3 days before collecting them for analysis.

Generation of shRNAs and lentiviral transduction

We purchased Perk or Atf4 specific shRNA-expressing lentiviral plasmid (Sigma-Aldrich) and produced lentivirus particles by transient co-transfection of 293 T cells as described [50]. After concentration of the lentiviral particles using a commercial Lenti-X concentrator (Takara Bio Inc, Shiga, Japan), we determined the titer of the concentrated lentivirus. We transduced secondary *Nf1*$^{fl/fl}$*;DhhCre* or *Runx1*$^{fl/fl}$*;Runx3*$^{fl/fl}$*;Nf1*$^{fl/fl}$*;DhhCre* DRG/neurofibroma cell derived spheres with purified shRNAs (sh*Perk* and sh*Atf4*) or non-target control lentivirus (Sigma-Aldrich). We incubated lentiviral particles with neurofibroma spheres at the multiplicity of infection (MOI) of 1:10–1:50 for 3 days and collected them for Western blot. For sphere number counting, we treated lentiviral particles at the MOI 1:10–1:50 for 4 days and counted sphere numbers [49].

Western blots

Mouse spheres or tumor tissues lysates were used for Western blots as described [49]. For immunoblotting, we used the following antibodies: anti-mouse PERK (#3192 S), p-PERK (#3179 S), IRE1α (#43294 S), ATF6 (#65880), p-eIF2α (#3398 S), ATF4 (#11815 S), ERK1/2 (#4695 S), p-ERK (#5726 S), CHOP (#5554 S), PARP (9542 S), XPO-1 (#46249), lamin B1 (#12586 S), GAPDH (#3683 S), β-actin (#5125 S) were from Cell Signaling Technology (Danvers, MA), p21 (#sc-6246) was from Santa Cruz Biotechnology, Santa Cruz, CA),and p-p21 (#E-AB-20947) was from Elabscience (Huston, TX). Antibody binding to the membrane was visualized using a chemiluminescent detection system (ECL, Millipore Sigma).

Immunoprecipitation assay

Mouse tissues were lysed in Np-40 buffer as described above, and 500–1000 μg of the total protein lysates were used for immunoprecipitation. The lysates were immunoprecipitated with anti-p21 (#sc-6246) antibody (Santa Cruz Biotechnology). The immunoprecipitated

complexes were resolved by SDS-PAGE and transferred to PVDF membranes for immunoblotting with Exportin-1/CRM1 antibody (#46249, Cell signaling Technology).

Tumorigenesis assay in nude mice

We subcutaneously injected 5×10^5 mouse sphere cells/injection within 33% matrigel into athymic nude mice flanks (males and females, Harlan, Indianapolis, IN) as described [49]. In the left flank, *Nf1*$^{fl/fl}$*;DhhCre* DRG/neurofibroma derived spheres, treated with 10 MOI NT control lentivirus, were injected. In the right flank, *Nf1*$^{fl/fl}$*;DhhCre* DRG/neurofibroma derived spheres, treated with 10 MOI sh*Perk* lentivirus, were injected. After 2 months, we dissected them to confirm visible tumors and counted the number.

Quantitative real-time PCR (qRT-PCR)

Total RNA was isolated from mouse tissues using the Qiagen RNeasy Kit (Hilden, Germany). The cDNA was synthesized using the High-Capacity cDNA Reverse Transcription Kit (Life Technologies, Carlsbad, CA). QRT-PCR was performed using SYBR Green (Applied Biosystems, Foster City, CA). The ΔΔCt method was used for calculation. Data represented at least three independent experiments with triplicate in each sample. The following mouse primers were used: *Gapdh, Grp78, Perk, Xbp1, Atf6, Rps17, Rps20, Rps23, Pde8a, Rpl31, Rpl11, Rps3, Rps7, Rps8, and Hprt* (Supplementary Table 1).

Protein synthesis assay

Protein synthesis assays were performed according to the Click-iT HPG Alexa Fluor 594 protein synthesis assay kit (ThermoFisher, #C10429) on cultured SCs. Briefly, mouse WT, *Nf1*$^{fl/fl}$*;DhhCre* or *Runx1*$^{fl/fl}$*;Runx3*$^{fl/fl}$*;Nf1*$^{fl/fl}$*;DhhCre* SCs (1×10^4 cells/well) were cultured in L-methionine-free medium containing 50 uM Click-iT HPG at 37 °C for 30 min and then the medium was removed. Cells were then fixed in 3.7% paraformaldehyde in PBS for 15 min, permeabilized in 0.5% Triton X-100 for 20 min, and washed in 3% BSA in PBS. Next, the cells were treated with Click-iT reaction cocktail for 30 min and then washed with Click-iT reaction rinse buffer. For nuclear staining, we added 1X HCS Nuclear Mask Bluestain solution for 30 min, and then we detected the staining results using fluorescence microscopy (Zeiss Axiovert 200 M, Carl Zeiss, Overcochen, Germany).

Immunohistochemistry and immunofluorescence

Formalin-fixed, paraffin-embedded tissue blocks were sectioned at 6 μm. Tissue sections were de-paraffinized in xylene, rehydrated in ethanol, and then boiled in citrate buffer for antigen retrieval. After blocking with 10% normal goat serum in TBST, the sections were incubated with primary antibodies: XPO-1, p21, PERK, or Ki67 (#12202 S, Cell Signaling Technology), overnight at 4 °C and then treated with biotinylated or Fluorescence dye-conjugated secondary antibodies for 1 h. The biotinylated antibody was detected with horseradish peroxidase-conjugated Streptavidin (Elite ABC, Vector Laboratories, Burlingame, CA) and cell nuclei were stained with hematoxylin. Fluorescently labeled sections were stained with DAPI (0.1 μg/ml) for nuclei counting and then mounted in Fluoromount G (Electron Microscopy Sciences, Hatfield, PA). Images were captured on a Nikon C2 Confocal microscope.

TUNEL assay

TUNEL assay was performed according to Roche In situ cell death detection kit instruction (#12156792910, TMR red, Roche Diagnostics Gmbh, Mannheim, Germany), on deparaffinized sections. We stained nuclei with DAPI. We counted TUNEL$^+$ cells and the DAPI nuclei in at least three cross sections per sample. Data were presented as an average percentage of TUNEL$^+$ cells per sample.

Statistics and power analysis

We used unpaired two-tailed Student's *t* tests to analyze the significance of tumor size, tumor number, and sphere number when two samples were compared. Other experiments used ordinary one-way or two-way ANOVA, represented as the mean ± SEM of more than three independent experiments. $P < 0.05$ was considered significant. For in vivo cell transplantation experiments, we used Fisher's exact test for power analysis and *P* value.

Supplementary Material

Refer to Web version on PubMed Central for supplementary material.

ACKNOWLEDGEMENTS

We thank Ms Bethany Bresnen for editing the figures. We also thank Mr Jonathan Rose for performing genotyping on some mice. This work was supported by NIH R01 NS097233 to JW and R01NS28840 to NR.

DATA AVAILABILITY

The materials described in the paper, including all relevant raw data, will be freely available to any researcher wishing to use them for non-commercial purposes, without breaching participant confidentiality.

REFERENCES

1. Blatt J, Jaffe R, Deutsch M, Adkins J. Neurofibromatosis and childhood tumors. Cancer 1986;57:1225–9. [PubMed: 3080222]
2. Boyd KP, Korf BR, Theos A. Neurofibromatosis type 1. J Am Acad Dermatol. 2009;61:1–14. [PubMed: 19539839]
3. McCormick F Ras signaling and NF1. Curr Opin Genet Dev. 1995;5:51–5. [PubMed: 7749326]
4. Le LQ, Parada LF. Tumor microenvironment and neurofibromatosis type I: connecting the GAPs. Oncogene 2007;26:4609–16. [PubMed: 17297459]
5. Ratner N, Miller SJ. A RASopathy gene commonly mutated in cancer: the neurofibromatosis type 1 tumour suppressor. Nat Rev Cancer. 2015;15:290–301. [PubMed: 25877329]
6. Varan A, Sen H, Aydin B, Yalcin B, Kutluk T, Akyuz C. Neurofibromatosis type 1 and malignancy in childhood. Clin Genet. 2016;89:341–5. [PubMed: 26073032]
7. Wang Y, Chen D, Qian H, Tsai YS, Shao S, Liu Q, et al. The splicing factor RBM4 controls apoptosis, proliferation, and migration to suppress tumor progression. Cancer Cell. 2014;26:374–89. [PubMed: 25203323]
8. Cubillos-Ruiz JR, Bettigole SE, Glimcher LH. Tumorigenic and Immunosuppressive Effects of Endoplasmic Reticulum Stress in. Cancer Cell 2017;168:692–706.
9. Hetz C, Chevet E, Oakes SA. Proteostasis control by the unfolded protein response. Nat Cell Biol. 2015;17:829–38. [PubMed: 26123108]

10. Oakes SA, Papa FR. The role of endoplasmic reticulum stress in human pathology. Annu Rev Pathol. 2015;10:173–94. [PubMed: 25387057]
11. Mohamed E, Cao Y, Rodriguez PC. Endoplasmic reticulum stress regulates tumor growth and anti-tumor immunity: a promising opportunity for cancer immunotherapy. Cancer Immunol Immunother. 2017;66:1069–78. [PubMed: 28577085]
12. Balch WE, Morimoto RI, Dillin A, Kelly JW. Adapting proteostasis for disease intervention. Science 2008;319:916–9. [PubMed: 18276881]
13. Deshaies RJ. Proteotoxic crisis, the ubiquitin-proteasome system, and cancer therapy. BMC Biol. 2014;12:94. [PubMed: 25385277]
14. Oromendia AB, Amon A. Aneuploidy: implications for protein homeostasis and disease. Dis Model Mech. 2014;7:15–20. [PubMed: 24396150]
15. De Raedt T, Walton Z, Yecies JL, Li D, Chen Y, Malone CF, et al. Exploiting cancer cell vulnerabilities to develop a combination therapy for ras-driven tumors. Cancer Cell. 2011;20:400–13. [PubMed: 21907929]
16. Clarke HJ, Chambers JE, Liniker E, Marciniak SJ. Endoplasmic reticulum stress in malignancy. Cancer Cell. 2014;25:563–73. [PubMed: 24823636]
17. Pollock PM, Harper UL, Hansen KS, Yudt LM, Stark M, Robbins CM, et al. High frequency of BRAF mutations in nevi. Nat Genet. 2003;33:19–20. [PubMed: 12447372]
18. Huber AL, Lebeau J, Guillaumot P, Petrilli V, Malek M, Chilloux J, et al. p58(IPK)-mediated attenuation of the proapoptotic PERK-CHOP pathway allows malignant progression upon low glucose. Mol Cell. 2013;49:1049–59. [PubMed: 23395000]
19. Hall A, Choi K, Liu W, Rose J, Zhao C, Yu Y, et al. RUNX represses Pmp22 to drive neurofibromagenesis. Sci Adv. 2019;5:eaau8389. [PubMed: 31032403]
20. Miller SJ, Jessen WJ, Mehta T, Hardiman A, Sites E, Kaiser S, et al. Integrative genomic analyses of neurofibromatosis tumours identify SOX9 as a biomarker and survival gene. EMBO Mol Med. 2009;1:236–48. [PubMed: 20049725]
21. Wu J, Williams JP, Rizvi TA, Kordich JJ, Witte D, Meijer D, et al. Plexiform and dermal neurofibromas and pigmentation are caused by Nf1 loss in desert hedgehog-expressing cells. Cancer Cell. 2008;13:105–16. [PubMed: 18242511]
22. Cichowski K, Shih TS, Schmitt E, Santiago S, Reilly K, McLaughlin ME, et al. Mouse models of tumor development in neurofibromatosis type 1. Science 1999;286:2172–6. [PubMed: 10591652]
23. Zhu Y, Ghosh P, Charnay P, Burns D, Parada L. Neurofibromas in NF1: Schwann cell origin and role of tumor environment. Science 2002;296:920–2. [PubMed: 11988578]
24. Chen C, Liu Y, Rappaport AR, Kitzing T, Schultz N, Zhao Z, et al. MLL3 is a haploinsufficient 7q tumor suppressor in acute myeloid leukemia. Cancer Cell. 2014;25:652–65. [PubMed: 24794707]
25. Choi K, Komurov K, Fletcher JS, Jousma E, Cancelas JA, Wu J, et al. An inflammatory gene signature distinguishes neurofibroma Schwann cells and macrophages from cells in the normal peripheral nervous system. Sci Rep. 2017;7:43315. [PubMed: 28256556]
26. Jessen WJ, Miller SJ, Jousma E, Wu J, Rizvi TA, Brundage ME, et al. MEK nhibition exhibits efficacy in human and mouse neurofibromatosis tumors. J Clin Investig. 2013;123:340–7. [PubMed: 23221341]
27. Williams JP, Wu J, Johansson G, Rizvi TA, Miller SC, Geiger H, et al. Nf1 mutation expands an EGFR-dependent peripheral nerve progenitor that confers neurofibroma tumorigenic potential. Cell Stem Cell. 2008;3:658–69. [PubMed: 19041782]
28. Axten JM, Medina JR, Feng Y, Shu A, Romeril SP, Grant SW, et al. Discovery of 7-methyl-5-(1-{[3-(trifluoromethyl)phenyl]acetyl}-2,3-dihydro-1H-indol-5-yl)-7H-p yrrolo[2,3-d]pyrimidin-4-amine (GSK2606414), a potent and selective first-in-class inhibitor of protein kinase R (PKR)-like endoplasmic reticulum kinase (PERK). J Med Chem. 2012;55:7193–207. [PubMed: 22827572]
29. Inoue Y, Kawachi S, Ohkubo T, Nagasaka M, Ito S, Fukuura K, et al. The CDK inhibitor p21 is a novel target gene of ATF4 and contributes to cell survival under ER stress. FEBS Lett. 2017;591:3682–91. [PubMed: 28975618]

30. Courtois-Cox S, Genther Williams S, Reczek E, Johnson B, McGillicuddy L, Johannessen C, et al. A negative feedback signaling network underlies oncogene-induced senescence. Cancer Cell. 2006;10:459–72. [PubMed: 17157787]

31. Abbas T, Dutta A. p21 in cancer: intricate networks and multiple activities. Nat Rev Cancer. 2009;9:400–14. [PubMed: 19440234]

32. Roninson IB. Oncogenic functions of tumour suppressor p21(Waf1/Cip1/Sdi1): association with cell senescence and tumour-promoting activities of stromal fibroblasts. Cancer Lett. 2002;179:1–14. [PubMed: 11880176]

33. Rodriguez JA, Span SW, Ferreira CG, Kruyt FA, Giaccone G. CRM1-mediated nuclear export determines the cytoplasmic localization of the antiapoptotic protein Survivin. Exp Cell Res. 2002;275:44–53. [PubMed: 11925104]

34. Ma Y, Hendershot LM. ER chaperone functions during normal and stress conditions. J Chem Neuroanat. 2004;28:51–65. [PubMed: 15363491]

35. Oakes SA. Endoplasmic reticulum proteostasis: a key checkpoint in cancer. Am J Physiol Cell Physiol. 2017;312:C93–C102. [PubMed: 27856431]

36. Croft A, Tay KH, Boyd SC, Guo ST, Jiang CC, Lai F, et al. Oncogenic activation of MEK/ERK primes melanoma cells for adaptation to endoplasmic reticulum stress. J Investig Dermatol. 2014;134:488–97. [PubMed: 23921951]

37. Sidoli M, Musner N, Silvestri N, Ungaro D, D'Antonio M, Cavener DR, et al. Ablation of Perk in Schwann Cells Improves Myelination in the S63del Charcot-Marie-Tooth 1B Mouse. J Neurosci. 2016;36:11350–61. [PubMed: 27807175]

38. Theocharopoulou G, Vlamos P. Modeling protein misfolding in charcot-marie-tooth disease. Adv Exp Med Biol. 2015;820:91–102. [PubMed: 25417019]

39. Bobrovnikova-Marjon E, Grigoriadou C, Pytel D, Zhang F, Ye J, Koumenis C, et al. PERK promotes cancer cell proliferation and tumor growth by limiting oxidative DNA damage. Oncogene 2010;29:3881–95. [PubMed: 20453876]

40. Nagelkerke A, Bussink J, Mujcic H, Wouters BG, Lehmann S, Sweep FC, et al. Hypoxia stimulates migration of breast cancer cells via the PERK/ATF4/LAMP3-arm of the unfolded protein response. Breast Cancer Res. 2013;15:R2. [PubMed: 23294542]

41. Feng YX, Sokol ES, Del Vecchio CA, Sanduja S, Claessen JH, Proia TA, et al. Epithelial-to-mesenchymal transition activates PERK-eIF2alpha and sensitizes cells to endoplasmic reticulum stress. Cancer Disco. 2014;4:702–15.

42. Koster R, di Pietro A, Timmer-Bosscha H, Gibcus JH, van den Berg A, Suurmeijer AJ, et al. Cytoplasmic p21 expression levels determine cisplatin resistance in human testicular cancer. J Clin Investig. 2010;120:3594–605. [PubMed: 20811155]

43. Zhou BP, Liao Y, Xia W, Spohn B, Lee MH, Hung MC. Cytoplasmic localization of p21Cip1/WAF1 by Akt-induced phosphorylation in HER-2/neu-overexpressing cells. Nat Cell Biol. 2001;3:245–52. [PubMed: 11231573]

44. Turner JG, Dawson J, Sullivan DM. Nuclear export of proteins and drug resistance in cancer. Biochem Pharm. 2012;83:1021–32. [PubMed: 22209898]

45. Cordonnier G, Mandoli A, Radhouane A, Hypolite G, Lhermitte L, Belhocine M, et al. CBFbeta-SMMHC regulates ribosomal gene transcription and alters ribosome biogenesis. Leukemia 2017;31:1443–6. [PubMed: 28196984]

46. Cai X, Gao L, Teng L, Ge J, Oo ZM, Kumar AR, et al. Runx1 Deficiency Decreases Ribosome Biogenesis and Confers Stress Resistance to Hematopoietic Stem and Progenitor Cells. Cell Stem Cell. 2015;17:165–77. [PubMed: 26165925]

47. Li H, Zhao X, Yan X, Jessen WJ, Kim MO, Dombi E, et al. Runx1 contributes to neurofibromatosis type 1 neurofibroma formation. Oncogene 2016;35:1468–74. [PubMed: 26073082]

48. Zhu Y, Romero MI, Ghosh P, Ye Z, Charnay P, Rushing EJ, et al. Ablation of NF1 function in neurons induces abnormal development of cerebral cortex and reactive gliosis in the brain. Genes Dev. 2001;15:859–76. [PubMed: 11297510]

49. Wu J, Keng VW, Patmore DM, Kendall JJ, Patel AV, Jousma E, et al. Insertional Mutagenesis Identifies a STAT3/Arid1b/beta-catenin Pathway Driving Neurofibroma Initiation. Cell Rep. 2016;14:1979–90. [PubMed: 26904939]

50. Arumugam PI, Scholes J, Perelman N, Xia P, Yee JK, Malik P. Improved human beta-globin expression from self-inactivating lentiviral vectors carrying the chicken hypersensitive site-4 (cHS4) insulator element. Mol Ther. 2007;15:1863–71. [PubMed: 17622240]

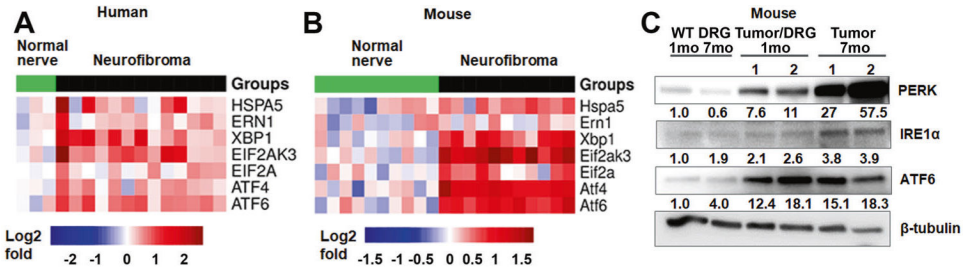

Fig. 1. ER stress-related genes are up-regulated in both human and mouse plexiform neurofibromas (PNFs).

A, **B** Heat maps showing differential expression of 7 ER stress-related genes in log2 fold in PNF tissue from NF1 patients (vs normal nerve) (**A**), or from *Nf1*$^{fl/fl}$*;DhhCre* mice at 7 months of age (vs age-matched WT mouse DRG) (**B**). **C** Western blot of 3 ER stress-related proteins in 1 month old DRG or 7 month old tumors from *Nf1*$^{fl/fl}$*;DhhCre* mice (vs DRG from age-matched WT mice); β-tubulin, loading control. Numbers indicated the relative fold change compared to WT controls.

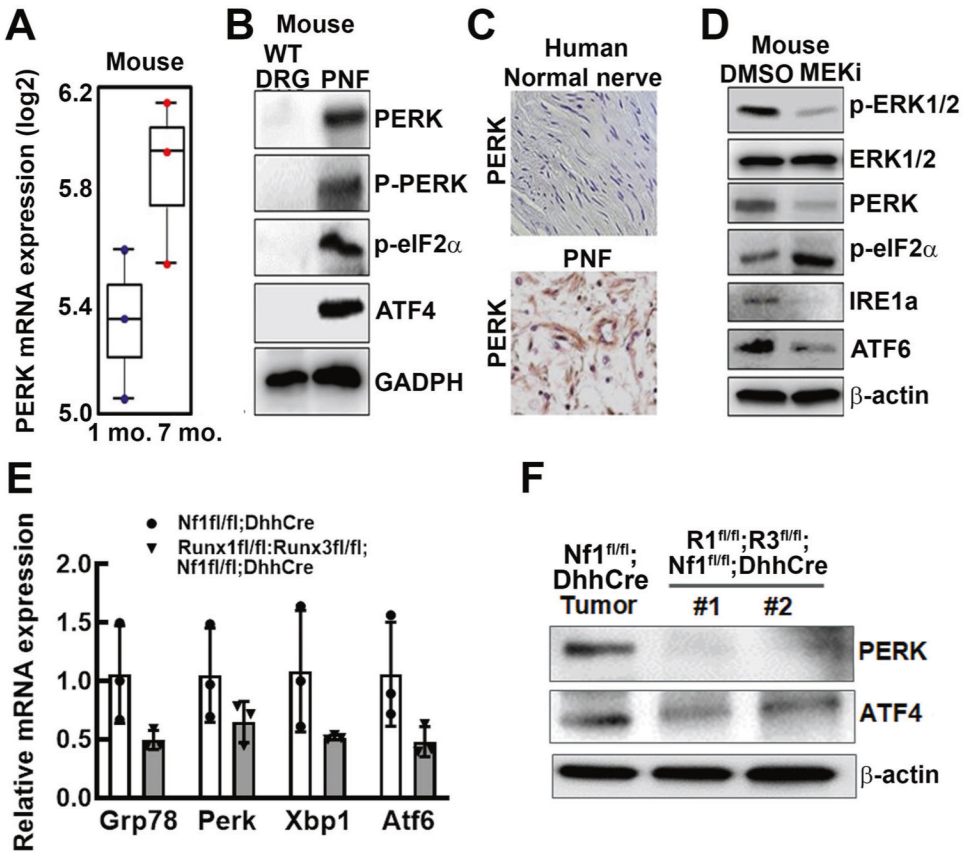

Fig. 2. PERK expression is increased in mouse and human PNFs and appears to be partially MEK/ERK and RUNX-dependent.

A Box and whisker plots showing relative mRNA expression in FACS-sorted SC from 1-month-old DRG (left) and 7-month-old mouse PNFs (right) ($n = 3$ mice/group). **B** Western blots of ER stress-related proteins (PERK, eIF2α, and ATF4 pathways) in mouse PNF vs age-matched WT DRG; loading control, GAPDH. **C** Representative DAB images of PERK (brown staining) IHC in human normal nerve (top) and PNF (bottom). Blue is hematoxylin and eosin counterstain for nuclei. **D** FACS-sorted mouse PNF SCs were treated for 24 h with MEKi (PD0325901, 1 μM) vs DMSO, and then Western blotted for proteins in all 3 ER stress pathways; loading control, β-actin. **E** QRT-PCR showing the relative mRNA expression of three ER stress pathway genes in *Nf1$^{fl/fl}$;DhhCre* (left, white bar) vs (*R1$^{fl/fl}$; R3$^{fl/fl}$; Nf1$^{fl/fl}$;DhhCre*, right, gray bar) $n = 3$ per group. **F** Western blot on tumors from *Nf1$^{fl/fl}$;DhhCre* and *Runx1$^{fl/fl}$;Runx3$^{fl/fl}$;Nf1$^{fl/fl}$;DhhCre* (*Rx1$^{fl/fl}$;R3$^{fl/fl}$;Nf1$^{fl/fl}$;DhhCre*). Loading control, β-actin. * = $p < 0.05$, ** = $p < 0.01$.

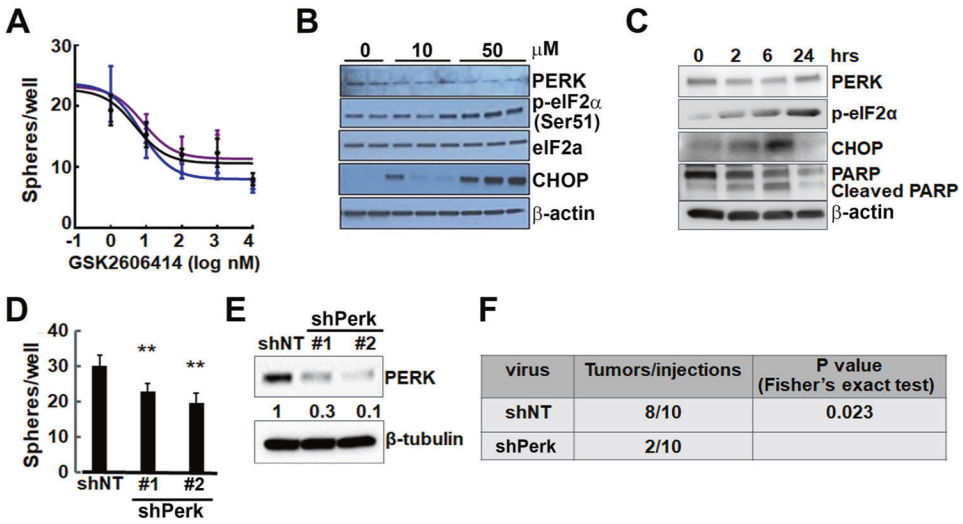

virus	Tumors/injections	P value (Fisher's exact test)
shNT	8/10	0.023
shPerk	2/10	

Fig. 3. PERK inhibition affects Schwann cell precursor growth or tumorigenesis.

A Decreased numbers of mouse neurofibroma-derived spheres by GSK2606414 treatment for 4 days. Three independent experiments were performed. Each line indicates one independent experiment with triplicates. **B**,**C** Inhibited PERK signaling and simultaneously induced apoptotic factors (cleaved PARP and CHOP) in mouse neurofibroma-derived spheres by GSK2606414 in dose response (**B**) and time course (**C**). **D** Significantly inhibited mouse neurofibroma sphere numbers treated by sh*Perk*-expressing lentivirus for 4 days. Experiments were performed in triplicates. **E** Efficiently inhibited PERK protein expression in mouse neurofibroma derived spheres as confirmed by Western blot. **F** Decreased tumor-like lesion formation rate by transplantation of sh*perk*-lentivirus treated sphere compared to that of sh*NT* control-treated sphere. A Fisher Exact test was performed. * = $p < 0.05$, ** = $p < 0.01$.

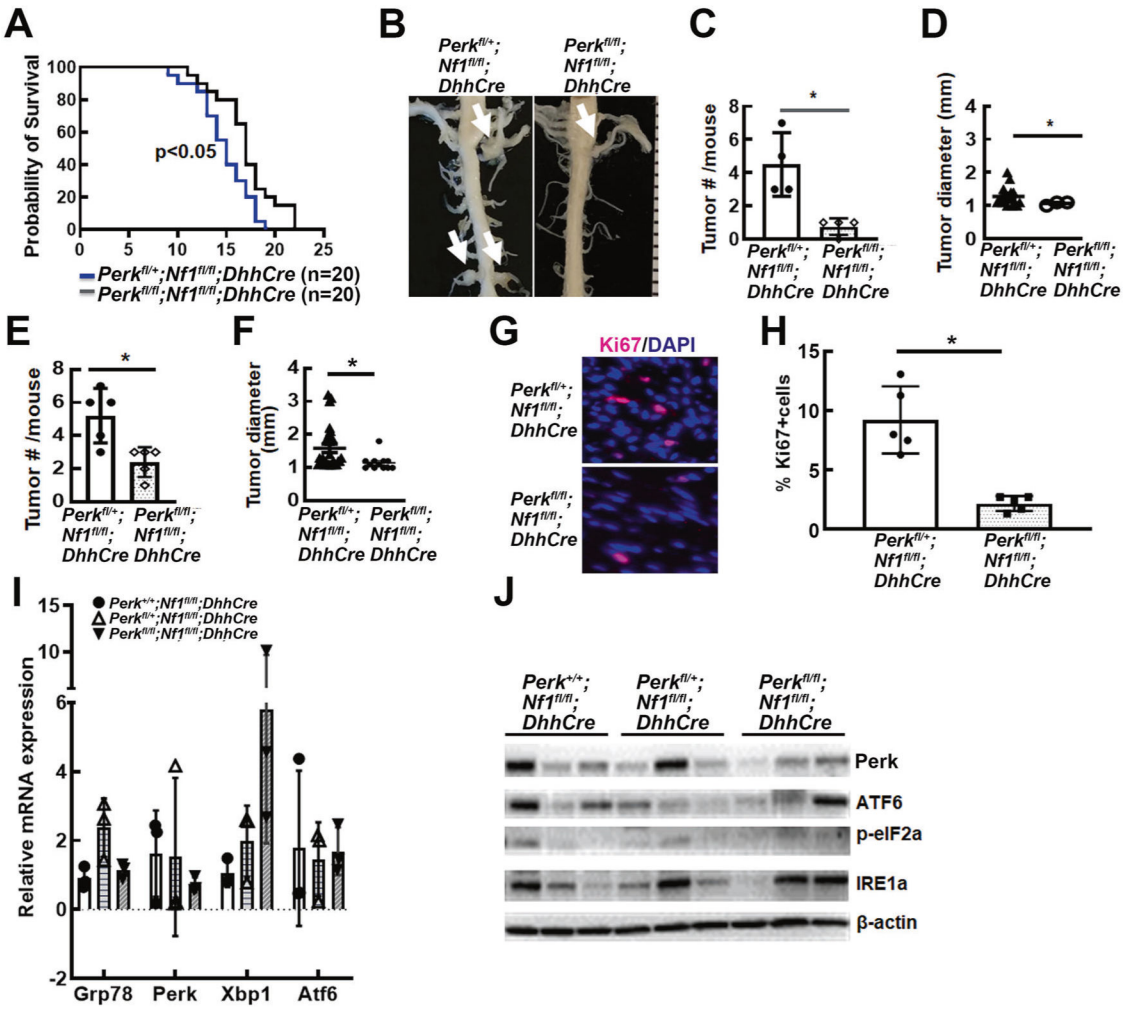

Fig. 4. Genetic deletion of PERK prolongs survival time and decreases tumor number and size in the *Nf1$^{fl/fl}$;DhhCre* PNF mouse.

A Kaplan–Meier survival curve. Black, *Perk$^{fl/fl}$;Nf1$^{fl/fl}$;DhhCre* mice ($n = 20$). Blue, littermates *Perk$^{f/l+}$;Nf1$^{fl/fl}$;DhhCre* mice ($n = 20$) ($p < 0.05$, log-rank test). **B** Representative gross dissections of thoracic paraspinal neurofibromas and nerve roots in 5 months of age-matched *Perk$^{f/l+}$;Nf1$^{fl/fl}$;DhhCre* (left) and *Perk$^{fl/fl}$;Nf1$^{fl/fl}$;DhhCre* (right). White arrows point to tumors. Ruler shows 1mm markings. **C**, **E** Average tumor number per mouse at 5 months (**C**, $n = 4$) and 12 months (**E**, $n = 5$) in the *Perk$^{f/l+}$;Nf1$^{fl/fl}$;DhhCre* mice (left, white bar) and *Perk$^{fl/fl}$;Nf1$^{fl/fl}$;DhhCre* mice(right, gray bar). **D**, **F**. Tumor diameter in the *Perk$^{f/l+}$;Nf1$^{fl/fl}$;DhhCre* mice at 5 (**D**. left, triangle, with 12 tumors) and 12 months of age (**F**. left, triangle, with 26 tumors) and *Perk$^{fl/fl}$;Nf1$^{fl/fl}$;DhhCre* mice at 5 (**D**. right, circle, with 3 tumors) and 12 months of age (**F**. right, circle, with 11 tumors). **G** Representative pictures of cell proliferation shown as Ki67+ cells (red) in *Perk$^{f/l+}$;Nf1$^{fl/fl}$;DhhCre* mice (top) and *Perk$^{fl/fl}$;Nf1$^{fl/fl}$;DhhCre* mice (bottom). DAPI (blue) was used to stain nuclei. **H** Quantification of percent of Ki67+ cells in *Perk$^{f/l+}$;Nf1$^{fl/fl}$;DhhCre* mice (left, white bar, $n = 5$) and *Perk$^{fl/fl}$;Nf1$^{fl/fl}$;DhhCre* mice (right, gray black bar, $n = 5$). * = $p <$ 0.05. **I** QRT-PCR in dot plots showing the relative mRNA expression of three ER stress pathway genes (*Grp78, Perk, Xbp1, and Atf6*) in *Perk^{+l+};Nf1$^{fl/fl}$;DhhCre* (left, white bar),

Perk$^{f/+}$;*Nf1*$^{fl/fl}$;*DhhCre* (middle, light gray bar) and *Perk*$^{fl/fl}$;*Nf1*$^{fl/fl}$;*DhhCre* mice (right, dark gray black bar) (n = 3 per group). **J** Western bots showing ER stress pathway related protein expression in tumors from *Perk*$^{+/+}$;*Nf1*$^{fl/fl}$;*DhhCre, Perk*$^{f/+}$;*Nf1*$^{fl/fl}$;*DhhCre* and *Perk*$^{fl/fl}$;*Nf1*$^{fl/fl}$;*DhhCre* mouse. n = 3 independent mice per genotype. Loading control: β-actin.

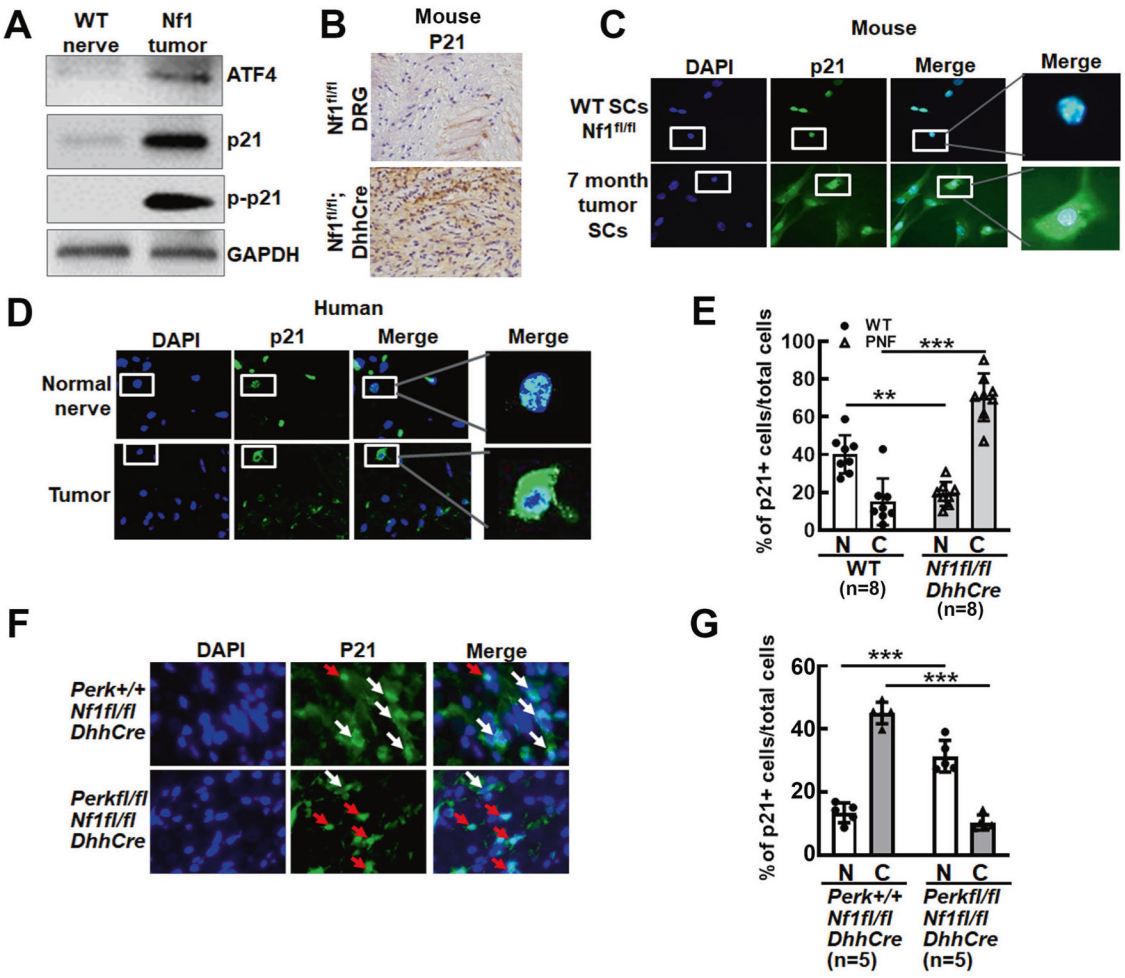

Fig. 5. Total p21 and cytoplasmic p21 expressions are increased in mouse and human PNFs.

A Western blot showing that ATF4, total p21 and phosphor-p21 (detecting cytoplasmic p21, p-p21) protein expression was increased in PNFs compared to controls. **B** IHC staining showing increased p21 expression (brown staining) in *Nf1*$^{fl/fl}$*;DhhCre* mouse PNFs (bottom) compared to WT DRG control (top). Blue is hematoxylin and eosin counterstain for nuclei. **C** Representative fluorescence images of p21 staining on WT mouse SCs (top) and 7 months *Nf1*$^{fl/fl}$*;DhhCre* mouse PNF-derived SCs (bottom). **D** Representative fluorescence images of p21 (green) staining on human PNFs. DAPI (blue) was used to staining nuclei. **E** Quantification of p21 percentage in nucleus (right, gray bar) or cytoplasm (right, gray bar) in human PNF (n = 8) vs normal nerve (n = 8, left, white bars). **F** Representative fluorescence images of p21 (green) staining on tumors from *Perk*$^{+/+}$*;Nf1*$^{fl/fl}$*;DhhCre* (top) and *Perk*$^{fl/fl}$*;Nf1*$^{fl/fl}$*;DhhCre* (bottom). White arrows point to cytoplasmic p21, red arrows point to nucleic p21. **G** Quantification of p21 percentage in nucleus (left, white bar, black circle) or cytoplasm (left, gray bar, black triangle) in *Perk*$^{+/+}$*;Nf1*$^{fl/fl}$*;DhhCre* tumors (n = 5) vs p21 percentage in nucleus (right, white bar, black circle) or cytoplasm (right, gray bar, black triangle) in *Perk*$^{fl/fl}$*;Nf1*$^{fl/fl}$*;DhhCre* tumors (n = 5). N: nucleus, C: cytoplasm. ** = p < 0.01, *** = p < 0.001.

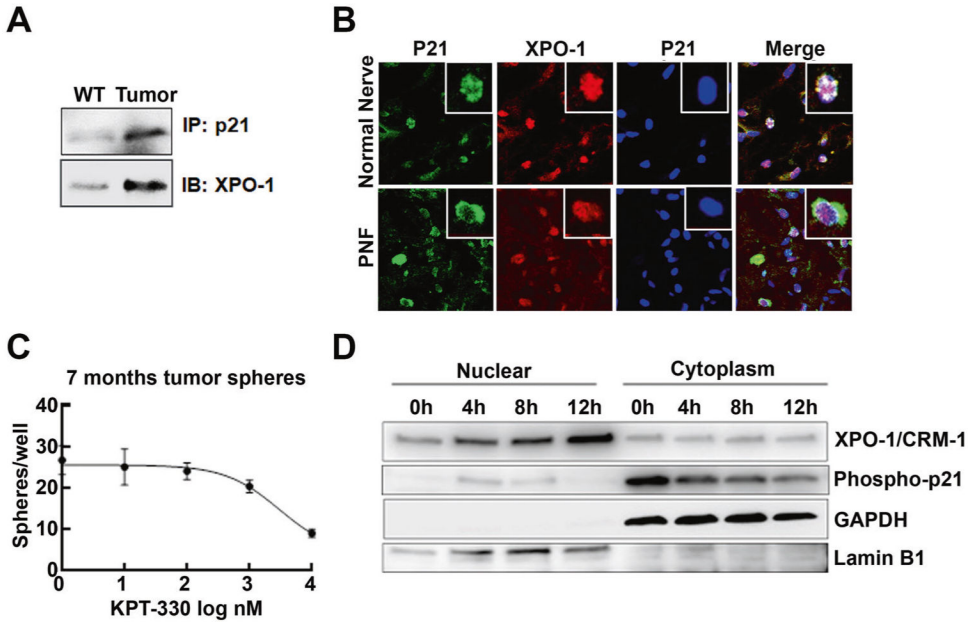

Fig. 6. Exportin-1 regulates p21 translocation from nucleus to cytoplasm.

A Interaction between Exportin-1 and p21 in 7 month-old mouse neurofibroma DRG/tumors. **B** Representative fluorescence images of p21 (green) and Exportin-1 (XPO-1, red) co-localization in human PNFs. DAPI (blue) was used to label nuclei. **C** Dose response curve showing decreased mouse neurofibroma-derived sphere numbers by treatment of Exportin-1 inhibitor, KPT-330. Three independent experiments were performed. **D** Time course showing conversely inhibitory effects of Exportin-1 and p21 in nucleus and cytoplasm by KPT-330 (5 μM).

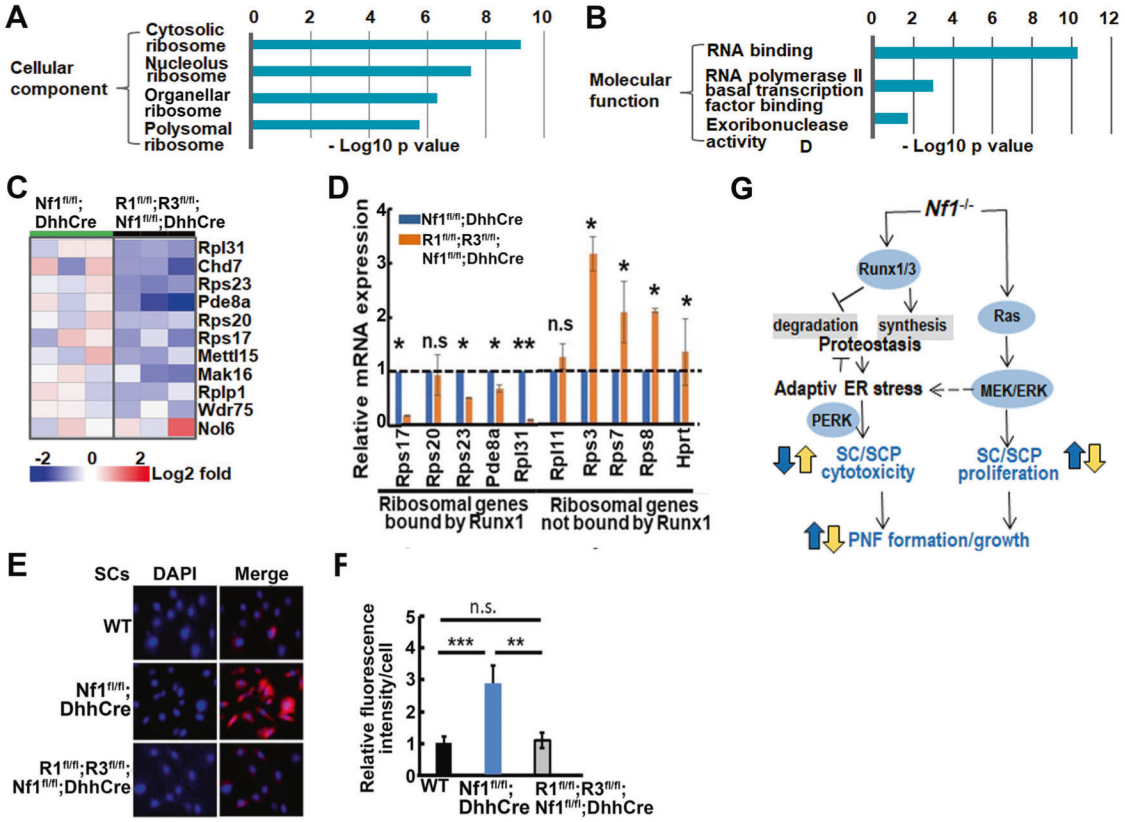

Fig. 7. Runx relates UPRs and protein synthesis in mouse neurofibromas with the regulation of ribosomal gene functions.

A,**B** Ontology analysis of Runx1-binding site in neurofibroma showing the involvement of ribosome in cellular component (**A**) and molecular function (**B**). **C** Decreased ribosomal gene expression in *R1*$^{fl/fl}$*; R3*$^{fl/fl}$*; Nf1*$^{fl/fl}$*;DhhCre* DRG/tumors by heat map RNA sequence compared to *Nf1*$^{fl/fl}$*;DhhCre* by log 2 fold change. **D** Decreased expression levels of Runx1-binding ribosomal genes in *R1*$^{fl/fl}$*; R3*$^{fl/fl}$*; Nf1*$^{fl/fl}$*;DhhCre* tissues compared to *Nf1*$^{fl/fl}$*;DhhCre* tissues ($n = 3$ per group). * = $p < 0.05$, ** = $p < 0.01$, n.s = no significant difference. **E** Increased protein synthesis rate in mouse neurofibroma SCs compared to WT SCs. Representatively decreased protein synthesis rates by Runx1/3 knock-out. **F** Quantification of relative fluorescence intensity/cell in cultures of SCs derived from either WT nerve (left, black bar) or PNFs from *Nf1*$^{fl/fl}$*;DhhCre* (middle, blue bar) or *R1*$^{fl/fl}$*; R3*$^{fl/fl}$*, Nf1*$^{fl/fl}$*;DhhCre* (right, gray bar). $n = 5$ per group. *** = $p < 0.001$. **G** In *Nf1*$^{-/-}$ SC/SCPs, Runx1/3 are elevated, which increases protein synthesis and might inhibit degradation, to maintain proteostasis, thereby inducing adaptive ER stress signaling to drive PNF formation and growth via PERK. SC Schwann cell. SCP Schwann cell precursor.